ChemElectroChem

Research Article
doi.org/10.1002/celc.202400465

Chemistry Europe
European Chemical Societies Publishing

www.chemelectrochem.org

Cost-Effective Solutions for Lithium-Ion Battery Manufacturing: Comparative Analysis of Olefine and Rubber-Based Alternative Binders for High-Energy Ni-Rich NCM Cathodes

Susan Montes,[a] Alexander Beutl,*[a] Andrea Paolella,[a, b] Marcus Jahn,[a] and Artur Tron*[a]

Promoting safer and more cost-effective lithium-ion battery manufacturing practices, while also advancing recycling initiatives, is intrinsically tied to reducing reliance on fluorinated polymers like polyvinylidene difluoride (PVDF) as binders and minimizing the use of hazardous and expensive solvents such as N-methyl pyrrolidone (NMP). In pursuit of this objective, olefin- and rubber-based polymers have been investigated as promising alternatives for binder materials in high-energy Ni-rich $LiNi_xCo_yMn_zO_2$ (NCM, $x \geq 0.8$) cathodes for lithium-ion batteries (LIBs). Alternative binders such as polyisobutylene (PIB), poly(styrene-butadiene-styrene) (SBS), nitrile butadiene rubber (NBR), and its hydrogenated version (HNBR) offer versatile solutions. These polymers can be dissolved in industrial solvents, such as toluene, and have been further processed into homogeneous cathode slurries, thus facilitating the manufacturing of high-energy Ni-rich NCM cathodes for lithium-ion batteries. The evaluation of NCM811 cathodes obtained from PIB, SBS, NBR, and HNBR has involved a thorough assessment of their physical and chemical properties, electrochemical performance, and production expenses, compared with NCM811 cathodes based on PVDF. Notably, cathodes employing PIB and HNBR have exhibited outstanding qualities, showcasing high specific capacity and remarkable electrochemical stability akin to PVDF-based counterparts. Furthermore, the alternative binders' superior adhesion, elasticity, and thermal stability have facilitated obtaining uniform and mechanically stable cathode films. Furthermore, using toluene, with its low vapor pressure, has significantly reduced energy costs associated with drying processes, thereby enhancing the overall cost-effectiveness of the NCM811 cathodes.

Introduction

Since their commercialization in the 1990s, lithium-ion battery (LIB) chemistries have had a high impact on our modern life, with currently growing markets for small- and large-scale applications.[1,2] To improve battery performance, there has been extensive and in-depth research into electrode materials,[3] coatings,[4] electrolytes,[5] additives,[6] membranes[7] and binders.[8]

Ni-rich layered oxides such as $LiNi_xCo_yMn_zO_2$ (NCM, where $x+y+z=1$ and $x \geq 0.8$), have recently attracted significant attention for their potential as cathode materials in high-energy LIBs. Its appeal lies in multiple advantages spanning theoretical capacity, operational potential, and production cost.[9] Nevertheless, despite advancements in the fabrication of Nickel-rich cathodes utilizing oxides like NCM811, significant hurdles persist in achieving cost-effective solutions for Lithium-ion battery manufacturing.[10] Challenges arise starting from the degradation of active material, alongside safety concerns related to overheating and overloads, caused by residual lithium compounds (RLC) originating from the choice of electrode materials, storage, and fabrication conditions.[11,12,13] Furthermore, enhancing cost-effectiveness and environmental sustainability by adopting fewer polluting materials, such as fluorine-free binders, while prioritizing occupational safety and health by opting for alternative solvents, are crucial steps to transition this technology from pilot lines to widespread commercial production and application in electric vehicles. Although binders in battery electrodes are often considered electrochemically inactive, they significantly influence the electrochemical performance and stability of the active materials.[14,15] The role of the binder in guaranteeing the cohesion of the electrode is essential. Despite its relatively minor mass contribution (2–5% by weight), the binder influences both the homogeneity and viscosity of the suspension, serving both as a dispersant and as a thickener.[16,17]

Binders also permeate the surface of active particles, establishing crucial bonds through mechanical entanglements and intermolecular forces. The presence of strong polar groups is also essential, as they improve the interfacial interaction with the particles and promote adhesion to the current collector. These bonds are vital to resist the stresses of the loading-

[a] S. Montes, A. Beutl, A. Paolella, M. Jahn, A. Tron
AIT Austrian Institute of Technology GmbH, Center for Transport Technologies, Battery Technologies, Giefinggasse 2, 1210 Vienna, Austria
E-mail: artur.tron@ait.ac.at
alexander.beutl@ait.ac.at

[b] A. Paolella
Università degli Studi di Modena e Reggio Emilia, Dipartimento di Scienze Chimiche e Geologiche, Via Campi 103, 41125 Modena, Italy

Supporting information for this article is available on the WWW under https://doi.org/10.1002/celc.202400465

unloading process, which requires flexible structures within the binder.[18] Equally significant is the thermal and electrochemical stability within the cycle voltage range. Thus, binders must withstand electrolyte corrosion and electrochemical reactions during operation to ensure optimal performance and safety. This stability is influenced by the binder's chemical composition, structure, and the surrounding chemical environment. Unstable binders can result in electrode failure and safety hazards. Therefore, the chemical stability of binders, alongside the electrode materials, electrolytes, and cyclic potential range, is a crucial factor in electrode design for achieving optimal electrochemical performance and stability. Polyvinylidene fluoride (PVDF) is a popular choice for binder material owing to its mechanical stability (tensile strength at break ~40 MPa at 23 °C),[19] crucial for preserving the structural integrity of the electrode throughout charge and discharge cycles. Its perceived chemical stability, coupled with its excellent binding capacity to both the active material and the current collector, makes it an attractive option for lithium-ion batteries. Additionally, PVDF facilitates easy lithium transport within the battery. However, it's worth noting that PVDF can undergo reactions with lithiated graphite and metallic lithium under elevated temperatures.,[20] and it tends to swell in organic solvents like ethyl carbonate (EC), diethyl carbonate (DEC), and dimethyl carbonate (DMC).[21] Moreover, PVDF undergoes reactions with lithiated carbon (Li_xC_6), resulting in exothermic heat generation and the formation of LiF and hydrogen on the electrode surface;[22] the deposition of LiF on the electrode surface contributes to capacity loss.[23] The use of PVDF as a binder in lithium-ion batteries (LIBs) may face regulatory scrutiny due to environmental concerns. European regulations, such as the REACH regulation, have classified perfluoroalkyl substances (PFAS), including certain fluorinated polymers such as PVDF, as substances of high concern.[24] While some advocate for PVDF to be considered "low concern polymers," others dispute this claim, citing potential environmental and health hazards. Additionally, rising prices and tight supply of PVDF highlight the need for alternative binder materials in LIBs. Despite its widespread use, the regulatory status of PVDF remains uncertain. The solvent N-methyl pyrrolidone (NMP) is widely used in cathode slurry coating due to its optimal suspension rheology.[25,26] Despite the availability of various organic solvents for PVDF, NMP stands out for its effectiveness in this application.[27] However, regulatory restrictions have been imposed on NMP due to its high toxicity.[28] Both the European Commission and the United States Environmental Protection Agency have limited their use under the REACH regulation and the Toxic Substances Control Act, respectively. These constraints highlight the need for alternative binders in LIB manufacturing processes, especially considering the environmental risks associated with recycling.[29] Reducing the use of PVDF as a binder, particularly in combination with toxic and costly NMP as an organic solvent, can lead to safer battery manufacturing and utilization. Efforts have been dedicated to exploring alternative binders enhancing the electrochemical performance of positive (cathode) and negative (anode) electrode materials in lithium-ion batteries (LIBs), while opting for more sustainable materials. Among these efforts, various materials such as carboxymethyl cellulose (CMC),[30] polyacrylic acid (PAA),[31] polyvinyl alcohol (PVA),[32] polymethyl methacrylate (PMMA),[33] PVDF-HFP,[34] and styrene-butadiene rubber (SBR)[35] have been investigated as binders for cathode films. SBR stands out due to its excellent chemical resistance, mechanical properties, good processability, and thermal stability, attributed to the rubber-olefin-based blocks in its polymer chain. Furthermore, the transition metal oxide cathodes (high nickel content materials, NCM) have been proposed for high theoretical capacity value and have been applied for small and large-scale applications.[36,37] However, these materials suffered from rapid capacity fade and high initial discharge specific capacity due to the enormous mechanical stress and pulverization during cycling life.[38,39] A lot of research and studies have been aimed at improving the electrochemical performance of NCM cathodes by various methods such as coatings,[40] additives,[41] electrolyte systems,[42] surface morphology[43] and particle size.[44] To improve the electrochemical performance of lithium-ion batteries, researchers have not only tried to harness the current or create new electrode materials. They have also searched for new binder systems to improve processability. Recently, other rubber- and olefin-based polymers like poly(acrylonitrile-co-butadiene) (NBR),[45] hydrated poly(acrylonitrile-co-butadiene) (HNBR),[46] poly(isobutylene) (PIB),[47] poly(butyl methacrylate) (PBMA),[48] poly(styrene-butadiene-styrene) (SBS),[49] and poly(styrene-ethylene-butadiene-styrene) (SEBS),[50] have gained attention for their fluorine-free nature. Tron and Beutl explored these polymers as binders in wet processing using p-Xylene as a solvent for sulfide-based solid-state electrolytes, showcasing their high electrochemical stability, ionic conductivity, and processability.[48,51] However, limited information exists on the application of these rubber- and olefin-based polymers as binders for electrode materials in LIBs. This study aims to investigate NBR, HNBR, PIB, and SBS for fabricating high-energy, Ni-rich cathode films for LIBs and compare them with PVDF films in terms of processability, costs, electrochemical performance, stability, and sustainability. Additionally, toluene is examined as a solvent, and its effects on the slurry are evaluated. The selection of binders and solvents used in this evaluation is depicted in Figure 1. The electrochemical performance of the fabricated electrodes is assessed through charge-discharge cycling, cyclic voltammetry, and electrochemical impedance spectroscopy. The analysis focuses on the electrochemical performance, its correlation with particle distribution in the films, adhesion with the current collector, formation of the solid electrolyte interface (SEI) layer, and the battery's performance under different C-rates, considering factors such as lithium diffusion and electronic conductivity.

Experimental

As ***cathode active material***, commercially available polycrystalline $LiNbO_3$-coated NCM811 ($LiNi_{0.8}Co_{0.1}Mn_{0.1}O_2$) was purchased from NEI Corp and stored in a glove box ($H_2O < 0.1$ ppm, $O_2 < 0.1$ ppm) until use. Carbon black (Super C65, Imerys) was used as a conductive additive and was stored until used in a drying oven at 100 °C.

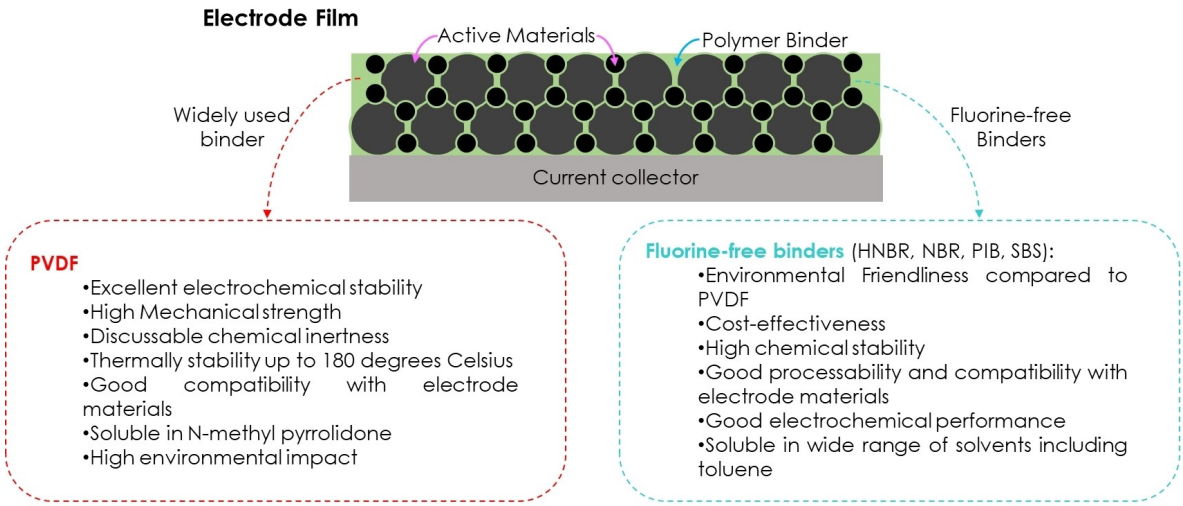

Figure 1. Comparison of PVDF and fluorine-free binders: Electrode film processing steps and material characteristics.

The ***Binders and Solvents*** that were used for the preparation of cathode suspensions as described in[48] are shown in Figure 2 and comparative physicochemical properties of the polymers used as binders are presented in Table S1. Poly(acrylonitrile-cobutadiene), also called nitrile butadiene rubber (NBR, Perbunan 1846F, Arlanxeo) denoted as P1, Poly(acrylonitrile-cobutadiene) hydrate (HNBR, Therban LT1707, Arlanxeo) denoted as T1, Polyisobutylene (PIB, OPPANOL N80, BASF, Mw ~800 000) denoted as O1, Poly(styrene-butadiene-styrene) (SBS, Sigma-Aldrich, Mw ~153 000–185 000) denoted as S1 and polyvinylidene fluoride (PVDF, Solef 5130, Solvay) were dried at 60 °C under vacuum for 24 h and stored in a glove box ($H_2O < 0.1$ ppm, $O_2 < 0.1$ ppm) until use. Anhydrous toluene (Sigma Aldrich) as well as N-methylpyrrolidone (NMP, Sigma-Aldrich) were used as received.

Binder solutions: The binder solutions were prepared by dissolving the polymers in their respective solvent (Figure 2) to form the solutions O1-Tol (14 wt/vol %), P1-Tol (8 wt/vol %), S1- Tol (8 wt/vol %), T1-Tol (7 wt/vol %) and PVDF-NMP (13 wt/vol %) by mixing the solvent and the binder in capped bottles at room temperature with magnetic stirring for 24 hours.

Electrode preparation: The cathode films were prepared by mixing the active material NMC811 (90% by weight) with carbon black as a conductive additive (5% by weight) with the respective binder (5% by weight using a mixer centrifugal planetary. (Thinky Mixer, ARE-250); The mass of active materials was approximately 8-9 mg cm^{-2} (loading of 1 mAh cm^{-2}).

After mixing, uniform slurries were obtained, with which the cathode films were manufactured. The films were formed by doctor blade method on current collectors of Al (Al, thickness = 15 μm)

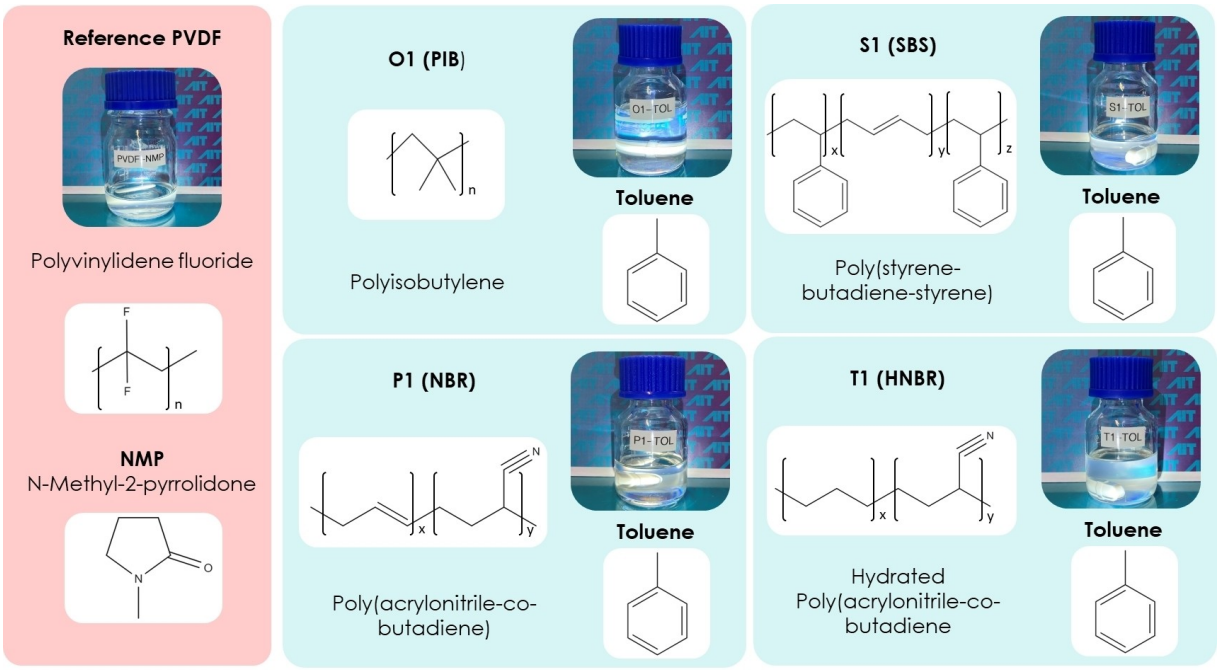

Figure 2. Binder and solvent selection for NMC811-based cathode film processing.

and carbon-coated aluminum foil (Al/C, thickness = 15 μm). The coatings were allowed to dry at room temperature under a fume hood for at least 10 minutes to remove excess solvent.

The films were subsequently dried in vacuum at different temperatures: NMC811-O1 (25 °C, 2 h; 80 °C, 2 h; 120 °C 2 h), NMC811-P1 (25 °C, 2 h; 80 °C, 2 h; 120 °C 2 h), NMC811-S1 (25 °C, 2 h; 80 °C, 2 h; 120 °C 2 h), NMC811-T1 (25 °C, 2 h; 25 °C, 2 h; 60 °C, 2 h; 80 °C, 2 h; 100 °C, 2 h; 120 °C, 2 h) and NMC811-PVDF (25 °C, 72 h; 120 °C, 8 h) as presented in Table S2. After drying, the electrodes were transferred to a glove box until use ($H_2O < 0.1$ ppm, $O_2 < 0.1$ ppm). The thickness of the electrodes was determined by measuring the thickness of circular slices (15 mm diameter) with a μm caliper. In order to ensure good inter-particle contact and reduce porosity, the electrode sheets were calendered. The electrodes with lower porosity could be produced by adjustment of the calender gap to smaller sizes - with a porosity of 70%. The electrode porosity was estimated by subtracting the total volume of all original components from the volume of prepared electrodes.

Electrochemical testing of cathode: For the electrochemical tests, the lithium metal anode (MTI, Li chips, diameter 15.6 mm, thickness 0.25 mm) was used as the counter electrode. The method used to prepare the lithium metal anode is described in.[51] The as-prepared electrodes were assembled in an argon-filled glovebox (< 0.1 ppm of H_2O and < 0.1 ppm of O_2) into CR2016 coin-type cells with NCM811 cathode active material as a working electrode, Li-metal foil as a counter electrode, polypropylene separator (Celgard 2500) and 1 M $LiPF_6$ in EC DEC 1/1 v/v (Aldrich) as electrolyte (as shown in Figure 3). The electrochemical tests were performed at 25 °C of the three cells for all samples (Figure S1, Supplementary Information). The cycling performance was investigated by MACCOR tester battery cycler in a potential range of 3.0–4.3 V at different current densities. Different C-rates (0.05 C, 0.1 C, 0.2 C, 0.5 C, 1 C and 2 C) were applied to cells to evaluate C-rate performance. Cyclic voltammetry (CV) measurements were conducted using the VMP potentiostat (Bio-Logic) at a scan rate of 0.5 mV s^{-1} in the potential range of 2.8–4.3 V (vs. Li/Li^+). Electrochemical impedance spectroscopy (EIS) measurement of used active materials in this work was performed on VMP potentiostat (Bio-Logic) with the frequency from 100 kHz to 100 mHz at a voltage amplitude of 5 mV.

Powder X-ray diffraction and Scanning electron microscopy: The obtained NCM cathode samples were determined by X-ray diffraction (XRD) analysis using a PANalytical X'Pert Pro diffractometer in Bragg-Brentano geometry with Cu Kα radiation (45 kV, 40 mA) in a 2θ range of 5–80° at a scan rate of 0.03° s^{-1}. The surface morphology of the samples was observed using field emission scanning electron microscopy (FE-SEM, ZEISS Supra 40) with energy-dispersive X-ray spectroscopy (EDS).

The Fourier transform infrared spectroscope and Raman analysis: The Fourier transform infrared spectroscope (FTIR, PerkimElmer UATR Spectrum Two) was detected within a wavenumber interval of 4000–400 cm^{-1} using a scan rate of 8 cm^{-1}. The Raman spectra were recorded at room temperature using a Xplora Plus confocal Raman microscope (Jobin-Yvon-Horiba). The microscope has a high-sensitivity CCD detector with thermoelectric cooling down to −60 °C for signal detection and a 532 nm laser as an excitation source.

Results and Discussion

The electrochemical performance of the olefine and rubber-based alternative binders for high-energy Ni-rich NCM cathodes of T1, P1, O1, and S1 electrodes was compared with the NCM811 electrode prepared by a traditional PVDF binder (Figure 2). Figure 4 and Figure S2 (Supplementary Information) show the rate performance of the NCM811 samples with binders as measured at various current densities of 0.05, 0.1, 0.2, 0.5 and 1 C each for five cycles in a potential range of 3.0 to 4.3 V (Li/Li^+). The PVDF sample displays a better rate capability compared to the T1, O1, P1, S1 samples can be attributed to the enhanced stabilized structure and surface morphology (Figures 5 and 7, and Figure S3, Supplementary Information). It should be noted that the cycling performance still needs to be improved, for example, by using various approaches such as changing structure, doping, coatings, additives for the organic electrolyte and using the "advanced" current collectors which can improve the surface morphology, mechanical stability and adhesion that can lead to enhance electrochemical performance.[40,41,42,43,44] The temperature treatment of samples can have a significant impact on the electrochemical performance. i.e., poor specific capacities before 80 °C due to remaining the Toluene solvent from cast and poor mechanical stability (Figure 5) that leads to increasing resistance values compared to the samples after 100 °C (Figure 4a). Therefore, after treatment of T1 samples after 100 °C, it was found that the T1 samples maintained higher electrochemical performance compared to the samples of 80 °C (Figure 4b). By comparison, the specific capacity of sample T1-120 (heat treated at 120 °C for 2 h) is higher than that of the PVDF electrode in the 50 cycles. While the T1-100 sample (heat treated at 100 °C for 2 h) maintains so close to the specific capacitances that the PVDF

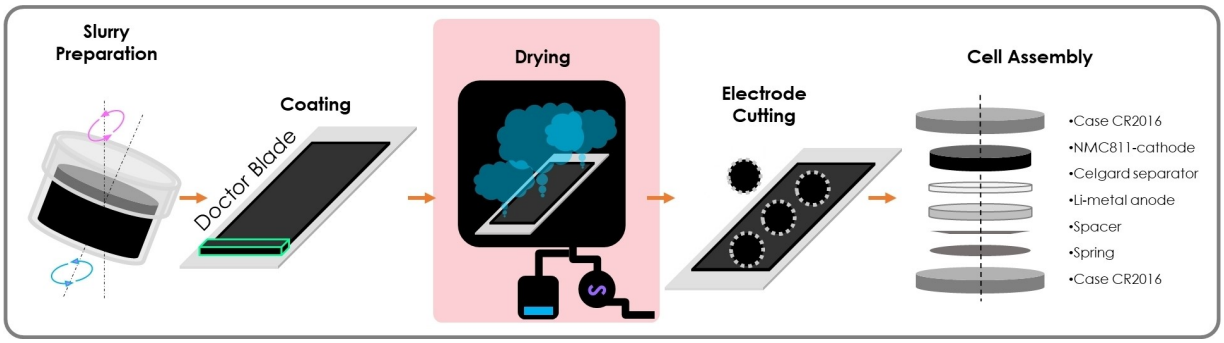

Figure 3. Schematic illustration of preparation and fabrication of cathodes with the following assembling in CR2016 coin cell configuration.

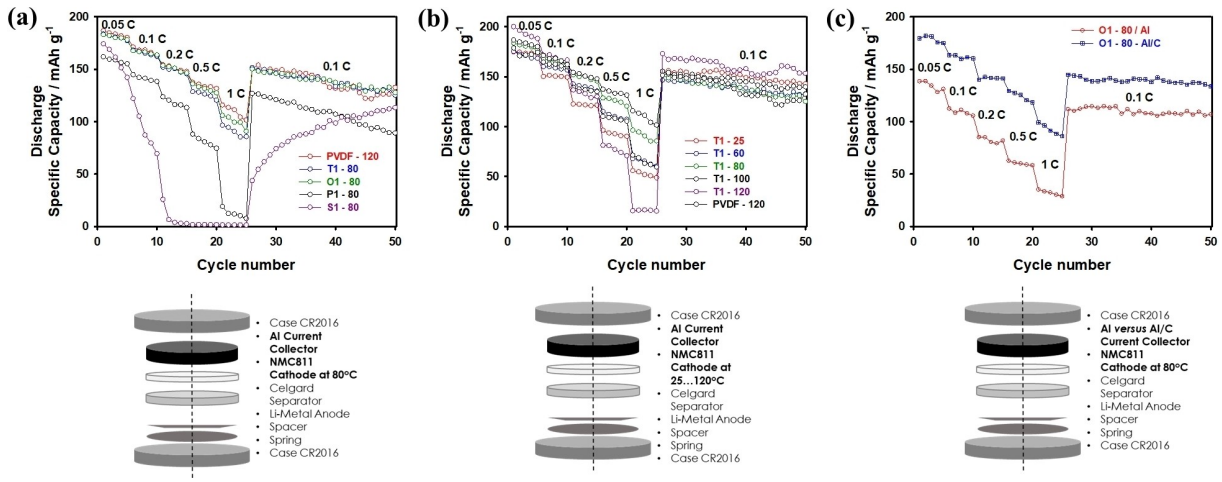

Figure 4. (a) The cycling performance of NCM811 samples (Al – current collector) fabricated via different binders PVDF-120 (heat treatment at 120 °C for 6 h), T1-80 (heat treatment at 80 °C for 2 h), O1-80, P1-80 and S1-80, (b) T1 binder after heat treatment at 25, 60, 80, 100, and 120 °C (Al – current collector), and (c) O1-80 (heat treatment at 80 °C) on Al and Al/C current collectors at different C-rates in the potential range of 3.0 V and cut-off potential of 4.3 V (vs. Li/Li^+).

sample at 120 °C. After 50 cycles, the average coulombic efficiency is 98% of the binder samples, which is an indication that the binders can improve the specific capacity of NCM electrodes. Obtained cycle data of T1 after temperature treatment at 100 and 120 °C can play the role of surface coating, firmly bonding electrode materials with stable and higher specific capacitances than PVDF sample (Figure 4b). The samples after the treatment at less than 80 °C have poor mechanical stability and cracks on the surface of the electrodes, which result in poor capacities (Figure 4a and Figure 5). Thus, the voltage attenuation issue of high nickel content materials can be effectively mitigated by using the olefine and rubber-based alternative binders at a temperature treatment above 100 °C and by using Al/C current collectors (Figure 4c and Figure S4, Supplementary Information). In addition, this superior rate capability of olefine and rubber-based alternative binder electrodes was attributed to the higher binding capacity and intrinsic ionic conductivity of these binders, resulting in the formation of a robust electrode structure and a highly distributed and interconnected electronic/ionic percolation network.

We expected that the surface changed because of the processability of NCM electrodes with various binders. To investigate in detail, the post-mortem SEM analyses before and after 50 cycles were conducted by SEM and cross-section images as shown in Figure 5. The surface morphology of the samples can directly reflect the bonding state between the electrodes after the preparation steps (Figure 3). Before cycling (Figure 5a), indicating that the PVDF and other binders (T1, O1, P1 and S1) can effectively bind the electrode components, the NCM active particles and conductive agents are evenly distributed on both electrode surfaces (Figure S5, Supplementary Information). While PVDF and other binder samples have such close surface morphologies with insignificant voids on the surface. However, T1 (HNBR) and S1 (SBS) samples show a denser inter-particle bond due to the homogeneous binder distribution and consequently homogeneous thickness of the prepared electrodes, whereas PVDF, O1 (NBR) and P1 (PIB) samples show pores after drying due to the more rapid evaporation of the solvent during drying of the cast electrode film.[48] It should be noted that a higher or lower degree of porosity can be expected depending on the amount of solvent used to prepare the electrode slurry (i.e. the solid content). Compared to the SEM images of samples after 50 cycles (Figure 5b), the gap between particles on the PVDF, T1 and P1 samples appears slight cracks that lead to poor cycle life. Noted, that PVDF binder plays a bonding role through the van der Waals force that causes its low bonding strength and limited bonding sites that result in the active particles easily falling off from the electrode during cycling with following capacity fading.[52] Regarding the T1, O1 and S1 binders after cycling, the particles of samples have still tightly bonded due to the strong hydrogen bonding between the binders and the lithium-rich active material except for the P1 sample which has a lot of particles on the surface is related to the solid content of the prepared slurries and the porosity of the cast electrode film and structural changes (Figure S6, Supplementary Information). However, to compare the drying temperature of T1 samples, T1 films after 100 °C have a smoother and denser surface due to the evaporation of remain Toluene solvent, although, the vapor pressure of Toluene (28.4 mm Hg at 25 °C) is quite higher than in NMP (0.342 mm Hg at 25 °C), and room temperature is enough for bonding strength between particles for fabrication of olefine and rubber-based alternative binders films (Figure S7, Supplementary Information), however for application of this solvent and binders needs to consider high temperature for interaction between particles and leads to the high cycling data (Figure 4c) and can play the role of the surface coating layer inhibiting the formation of side reaction components during the cycling.[48,53] Moreover, it was found that Al/C current collector can have a positive role in firmly bonding the electrode material to the current collector and inhibit the separation of the active particles from the electrode during fabrication and cycling as shown in Figure 4c and Figure 5c. In

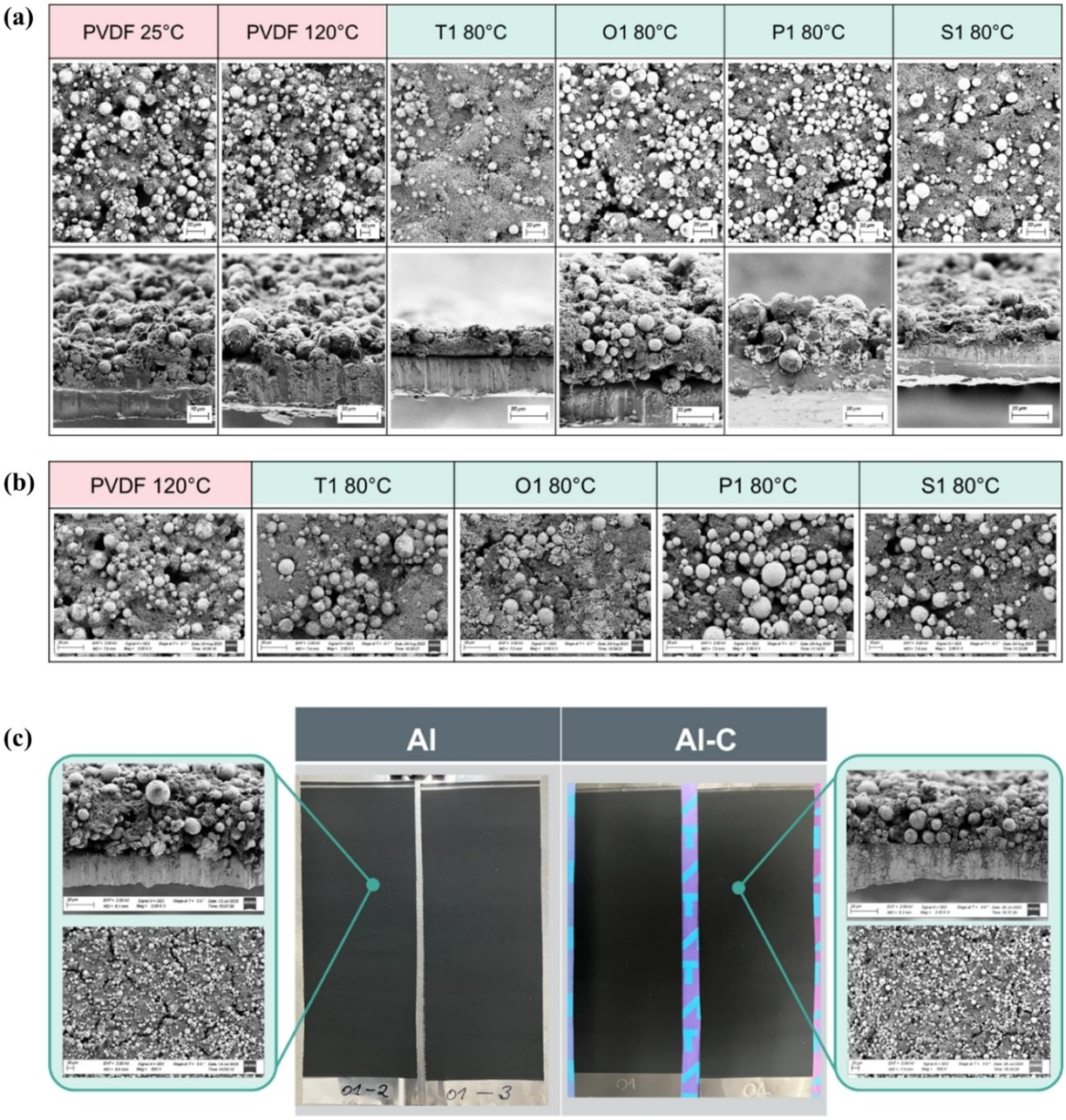

Figure 5. SEM and cross-section images of NCM811 surface cathodes (a) before and (b) after cycling with PVDF-25 (heat treatment at 25 °C for 72 h), PVDF-120 (heat treatment at 120 °C for 6 h), T1-80 (heat treatment at 80 °C for 2 h), O1-80, P1-80 and S1-80 samples after heat treatment, and (c) Surface analysis of NCM811 cathode with O1 (PIB) binder on the top of aluminum (Al) and aluminum-carbon (Al/C) current collectors.

addition, when with the amount is low (1.5 wt%) the electrode exhibit a lower electrochemical performance due to the contact between current collector and cathode layer (Figure S8, Supplementary Information). Thus, we can conclude that good structural integrity is the key factor for the excellent electrochemical performance of the NCM electrodes with binders used in fabricating sulfide solid-state batteries. Furthermore, the cross-section morphology of the samples can reveal the degree of adhesion between the electrode material and the current collector before and after cycling as shown in Figure 5. Compared to the other binders, the PVDF electrode material is relatively well bonded to the Al current collector before cycling. However, to improve the good adhesion between the current collector and the cast, the Al/C current collector was used, which resulted in good contact with excellent electrochemical performance and lower resistance (Figure 4c). During the cycle, the separation between the cast and the Al current collector is obvious, indicating a poor adhesion role of the olefine and rubber-based alternative binders, which is insufficient to resist the load, maintaining mechanical instability and poor performance (Figure 4a and 4b). Note that the use of these bonding agents in the manufacture of cathode laminates in combination

with Toluene solvent, due to the higher vapor pressure than water and NMP, avoids the corrosion effect of the current collectors compared to water solvent and provides a robust bond between the cathode layer and the current collectors that can resist the mechanical stress encountered during cell manufacture and cell cycle[35] and (as shown in Figure 4 and 5).

It is also necessary to understand the binding mechanisms to verify the influence of olefine and rubber-based alternative binders on cathode performance. The binding capacity of PVDF is mainly achieved by physicomechanical interactions, which are relatively weak compared to the chemical bonds formed between the S1 and O1 binders and the active material, resulting in lower electrochemical performance (Figure 4). T1 and P1 resins have stronger binding due to the condensation reaction of bonds with surface functional groups of electrode materials, leading to good adhesion. The O1 binder on the Al/C current collector has a higher binding capacity to effectively limit electrode laminate delamination and maintain electrode integrity during cell cycling compared to the O1 sample on the Al current collector (Figure 4c). For a better understanding of the adhesion properties of the binders, a peel test experiment was measured as shown in Figure S9 (Supplementary Information). The olefine and rubber-based alternative binders (T1–6 N, O1–6 N, P1–8 N and S1–37 N) were found to have higher peel strength than the PVDF binders. Note that the resin had the highest value of 15 N, which is almost higher than the resin and PVDF and may explain the stable electrochemical performance as shown in Figure 4.

The EIS spectra before and after cycling of the PVDF and T1, O1, P1, S1 samples are shown in Figure 6. The Nyquist plots are obtained with a semicircle in the high to medium frequency region, which corresponds to the surface resistance to the transport of lithium through the surface film and the charge transfer between the organic liquid electrolyte and the electrode materials. The low-frequency region is attributed to an inclined line that corresponds to the diffusion of lithium ions in/out of the NCM structure.[54] The equivalent circuit shown in the inset of Figure 6a was used to fit the impedance spectra. R_e is the resistance of the organic liquid electrolyte and $R_{surface}$ is the surface ion transport resistance associated with the redox reaction of lithium ions into/out of the structure of NCM; can be attributed to the formation of an insulating solid electrolyte interphase (SEI) layer or the deposition of organic electrolyte compounds.[55,56] A constant phase element (CPE) has been used instead of a pure capacitor, which is placed in parallel with the surface resistance ($R_{surface}$) and in series with a further Warburg impedance. The PVDF and T1, P1 samples have a lower resistance ($R_{surface}$) than O1 and S1 before and after cycling (Figure 6c). T1, P1 and S1 have denser surfaces and good mechanical stability (Figure 5) which can mitigate or stabilize the resistance increase, making lithium reactions fast with good electrochemical performance (Figure 4). It should be noted that, unlike the case of organic electrolytes, the conventional SEI layer is generally not formed in the aqueous electrolyte.[57,58] Therefore, the samples O1 (PIB) have an additional semi-circuit that can occur through the electrolyte/electrode interface due

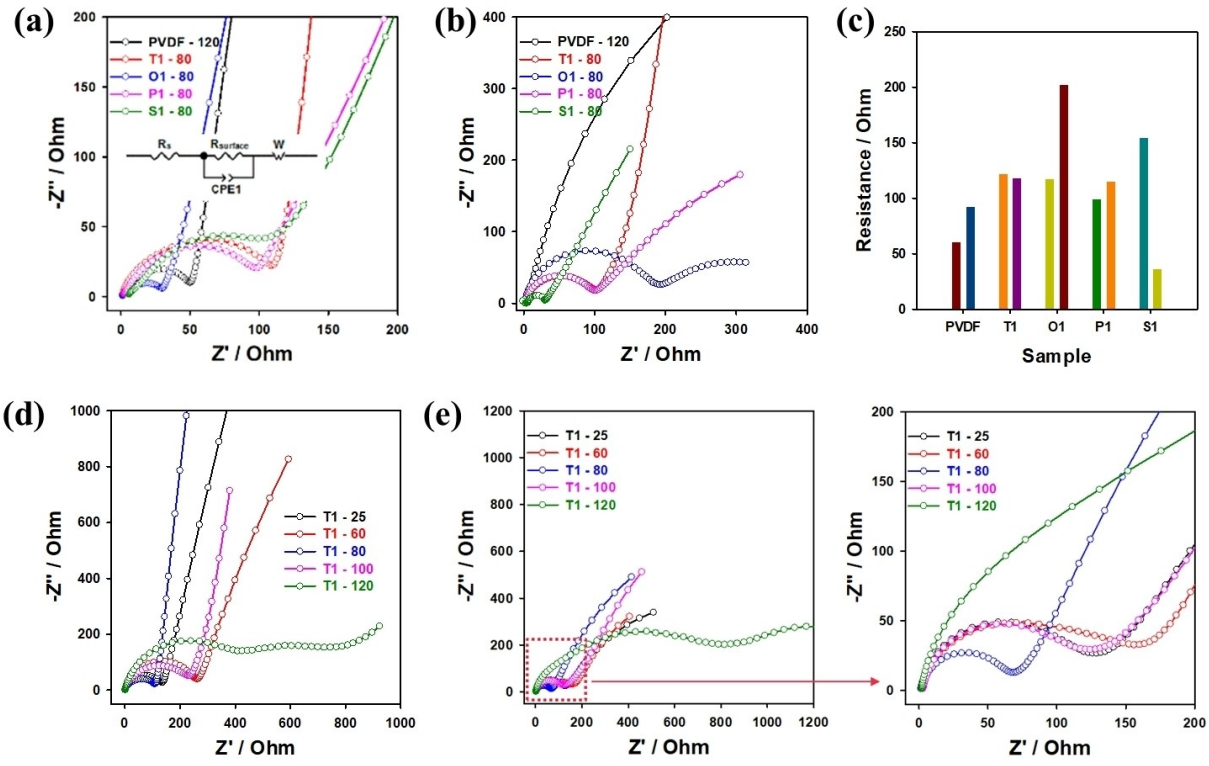

Figure 6. Nyquist plots of NCM811 surface cathodes (a) before, (b) after cycling with PVDF, T1, O1, P1 and S1 binders, (c) Resistance of samples after heat treatment (where B – before, A – after cycling), and NCM samples with T1 at various heat treatment (d) before and (e) after cycling in the organic electrolyte of 1 M $LiPF_6$ in EC DEC (1:1. v/v) in the potential range of 3.0–4.3 V at 25 °C.

to the passivation layer or possible side reaction components formed on the surface of the NCM electrodes, leading to lower electrochemical performance (Figure 4). By contrast, the temperature treatment after 100 °C can have an impact on the increasing of resistance values compared to the 80 °C and can lead to improve electrochemical performance due to the evaporation of the Toluene solvent from cast and better mechanical stability as discussed above (Figure 6d and 6e). Compared to O1 and S1 samples, T1 and P1 samples exhibited lower and decreasing interfacial resistances during cycling (Figure 6c), as the surface coverage effectively protected the active material from electrolyte attack. Furthermore, an increase in the charge transfer resistance of O1 and S1 was observed. This could be due to the degraded Li^+ diffusion during cycling. In addition, T1 and P1 on the Al current collector exhibited the lowest impedance values due to the stable surface conductivity (the intrinsic ionic conductivity), facilitating faster lithium transport during cycling. Thus, it can lead to the prevention of electrolyte decomposition on the active material surface and the reduction of cathode polarisation (Figure S2 and Figure S4, Supplementary Information).

To show the structural changes of NCM electrodes with different binders after heat treatment before and after cycling (Figures 7a and 7b). It should be noted that the temperature evaporation of the solvent has a great influence on the structural changes and can lead to the collapse or change of the peak intensity of the NCM811 structure, with the following characteristic peaks corresponding to the layered NCM cathode being greatly changed compared to the NCM powder. For example, the intensity of (003) was much lower than that of (104), and the Li^+/Ni^{2+} cation mixture increased significantly for T1, O1 and P1 samples treated at 80 °C before and after cycling.[59] However, after treatment above 100 °C, the structure of the binders was not much different (Figure 7 and Figure S10, Supplementary Information). Moreover, the splits for the (006)/(012) and (018)/(110) peaks confirmed a well-ordered layered structure for all samples, without any bulk changes in the crystal lattice in the obtained samples, only with lower intensities of the peaks related to the formation of the SEI layer and the increase in resistance for olefine and rubber-based alternative binders (Figures 5 and 6). It should be noted that the temperature treatment in the preparation process (Figure 2) can have an impact on the structural and morphological

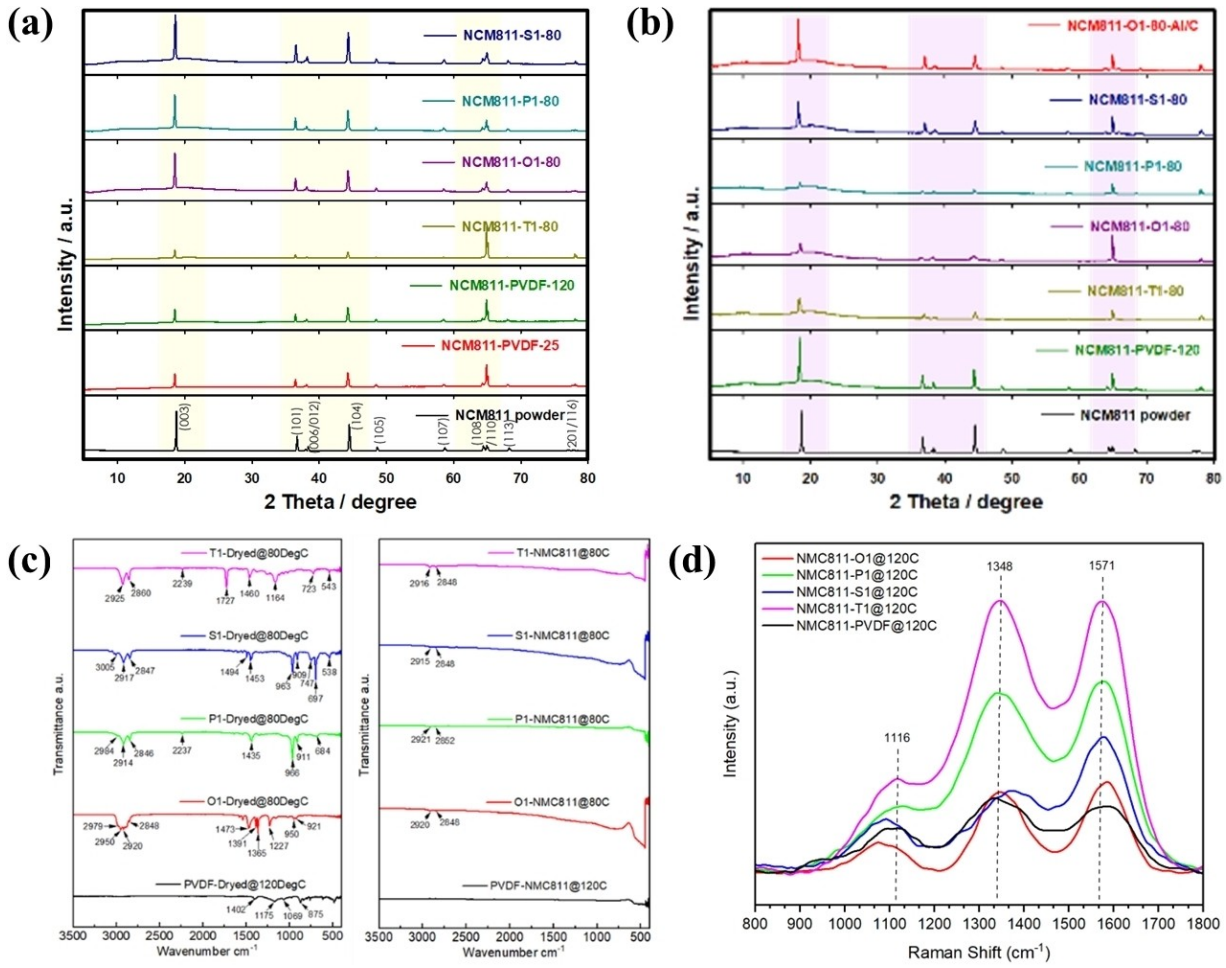

Figure 7. XRD patterns of NCM811 surface cathodes (a) before, (b) after cycling with PVDF, T1, O1, P1 and S1 binders in the organic electrolyte of 1 M $LiPF_6$ in EC DEC (1 : 1. v/v) in the potential range of 3.0–4.3 V at 25 °C, and (c) FTIR spectra of binders and NCM electrode films and (d) Raman spectra of NMC811-electrode films coated on aluminum current collectors.

changes. In addition to structural and morphological changes, Fourier Transform Infrared (FTIR) spectroscopy of the surface of binders and NCM electrode films was performed to understand the difference in improving the electrochemical reactivity of different binders, as shown in Figure 7c. In addition, for T1, S1, P1 and O1, relatively strong absorption bands at 900 and 1000 cm^{-1}, and 3000 and 2800 cm^{-1} can be attributed to the ether linkage. Several groups are superimposed in the vicinity of the 1400 cm^{-1} wave number, including aldehyde groups, ester groups, carboxyl groups and other groups. However, the others are not easily oxidized, which has a good effect on the resistance of the as-prepared binders and NCM cathode composite films. On the other hand, for the PVDF binder, the absorption peaks at 1175 and 875 cm^{-1} are due to the vibration of the CF2 bond and the characteristic peaks of the CH2 and C–C bonds are at 1402 and 1175 cm^{-1}, respectively. Furthermore, some sharp peaks around 1175, 1069 and 875 cm^{-1} are assigned to PVDF phase peaks, indicating crystalline structure changes in the PVDF binder. Raman spectroscopy (Figure 7d) was used to monitor local structural changes in NCM cathodes with binders after cycling. The characteristic of the structural changes that occur during cycling, PVdF shows three prominent bands at 1116, 1348 and 1571 cm^{-1}. In contrast, the cycled T1, S1, P1 and O1 still show the original spectral features of the pristine material, which can lead to more stable structural and morphological changes. It should be noted that thermal stability is a critical property of polymer binders using in LIBs. As their typical operating temperature range remains below 60 °C, polymer binders can be exposed to higher temperatures over 100 °C during the manufacturing process, which can lead to an increase in their battery operating temperature.[60] Most cross-linked and cyclic polymers have increased thermal stability compared to conventional PVdF binders, which tend to loosen or weaken at high temperatures, reducing the mechanical strength required to hold the active, conductive and current collector together.[61] Therefore, the thermal analysis of the use of binders for cathode materials was carried out in this work. It was found that fluorine-free binders maintain thermal stability compared to PVDF binder (Figure S11, Supplementary Information). In addition, obtaining the thermal results may influence the intra- and intermolecular interactions between polymeric binders and cathode components, affecting their structures and significantly altering their thermal stability, which may help to maintain the stability of the electrochemical performance (Figure 4). For example, due to the residual toluene solvent in the samples, the formation of agglomeration can lead to the exposure of the material for P1 and the formation of a thick SEI layer on the surface, allowing the internal material to come into direct contact with the organic electrolyte, with further capacity degradation. Therefore, when comparing the cycling results obtained, the samples treated above 100 °C were better in terms of electrochemical performance than those treated at 80 °C (Figure 4).

Figure 8 shows the CV curve of binder samples, which may reflect the redox reaction of NCM electrodes during charging and discharging. The CV curves of all binder samples have similar redox peaks and correspond to the oxidation reaction of transition metal ions Ni^{2+}/Ni^{4+} and Co^{3+}/Co^{4+} at a potential range of 4.0 to 4.3 V.[62] The peaks between 3.7 and 3.8 V are related to the reduction of Mn^{4+}/Mn^{3+} and the structural transformation from a layered to a spinel phase structure. It should be noted that in these peaks for O1 (NBR) and P1 (PIB) - Mn^{4+}/Mn^{3+} disappears, which can be related to the structure of the binder and the formation of a thick SEI film on the surface of the NCM electrodes and is consistent with the cycling life and can maintain structural stability (Figures 4 and 5).

Obtained the coefficient diffusion of T1, O1, P1, and S1 binders samples have so close to the value with PVDF sample

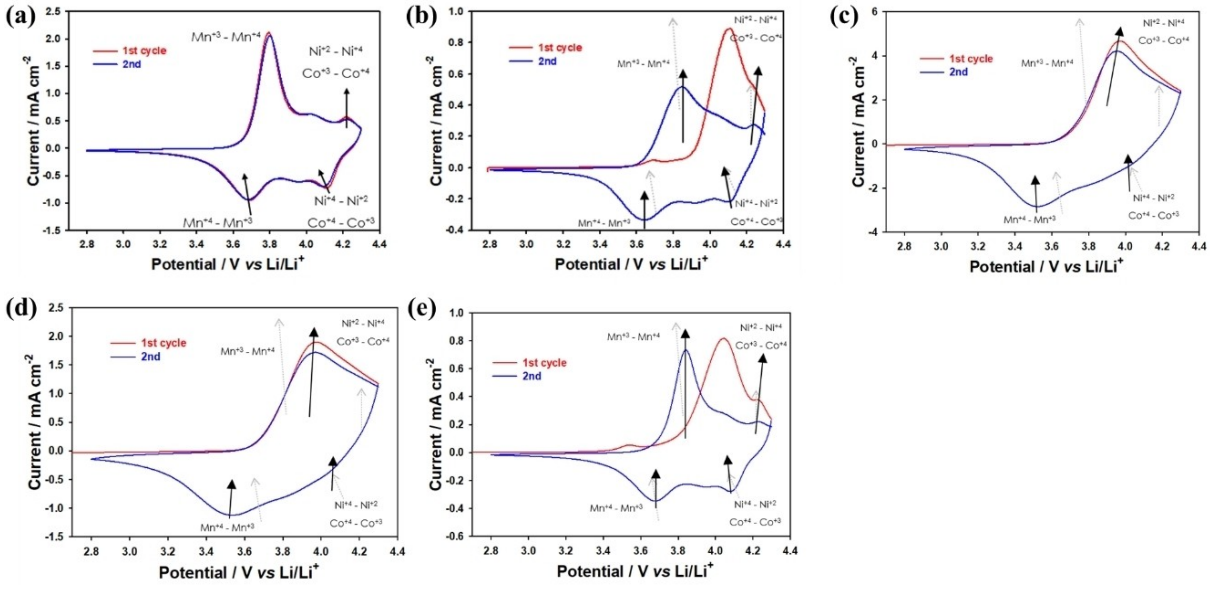

Figure 8. Cyclic voltammetry in the potential range of 3.0–4.3 V at a scan rate of 0.5 mV sec^{-1} of NCM811 cathode material in the organic electrolyte of 1 M $LiPF_6$ in EC DEC (1 : 1, v/v) with (a) PVDF, (b) T1, (c) O1, (d) P1 and (e) S1 binders.

that can give a positive in using these binders as alternative candidates for lithium-ion battery cathode materials (Table 1). Although some binders compared to the PVDF sample have structural deterioration of cathode materials and can hinder the ion migration paths and lead to capacity fading. However, after proposition in the improvement of the fabrication of electrodes via temperature treatment, using the Al/C current collectors, we can conclude that this strategy can help in maintaining stable electrochemical performance (Figure 4b and 4c). Moreover, the T1 and S1 exhibit higher coefficient ion diffusion abilities than PVDF and O1, P1, which reflects their structural instability and can hinder the intercalation/deintercalation of Li ions leading to damaging the reversible capacity of the NCM811 electrodes.

The change in kinetics at the electrode/electrolyte interface after storage is investigated by EIS during the 30 days as shown in Figure 9. The EIS data obtained for the T1 binder show no obvious difference in the electrolyte resistance and surface film resistance compared to the PVDF, O1, P1 and S1 samples. This evidence can be related to the H1 phase and the H2-H3 phase transition in the low potential region (3.00-3.80 V) and the high potential region (4.15–4.30 V) respectively.[63,64] Furthermore, the R_{ct} values increase significantly with increasing storage time, which can be attributed to the structural instability of the electrodes and the formation of side reaction components on the electrode surface, which hinder lithium transport. It is concluded that the interfacial charge transfer kinetics of the H1 phase is relatively slow, which may lead to lower electrochemical performance.[65]

Table 1. Coefficient diffusion of NCM cathode samples with different binders.

Sample	Coefficient diffusion (EIS) of NCM electrode
PVDF-120	$1.28\ 10^{-11}$
T1-80	$2.38\ 10^{-12}$
O1-80	$3.64\ 10^{-11}$
P1-80	$1.79\ 10^{-11}$
S1-80	$4.59\ 10^{-12}$

In this work, we are considering investigating the transparent LCA for binders used for the fabrication of NCM811 electrode from the point of view of understanding the life cost assessment for assembling lithium-ion batteries and compared to the conventional PVDF-based NCM electrodes. The cost of electrode fabrication is reduced directly by exchanging the PVDF-NMP polymer solution by cheaper polymer solutions T1-toluene, O1-toluene, P1-toluene and S1-toluene. The use of toluene as solvent reduces the drying time from 8 to 2 hours and allowing to dry electrodes at lower temperatures, reducing the cost of electrical energy to operate drying ovens (Figure 10). The improvements that can be achieved over the existing conventional PVDF-based positive and negative electrode materials of LIBs are promising, considering the low technical use of olefine and rubber-based alternative binders for lithium-ion battery chemistries. However, the fundamental and economic benefits of these binders for their future application in LIBs are still an open question. In addition, the cost of LIB components is a function of the high cost of raw materials and

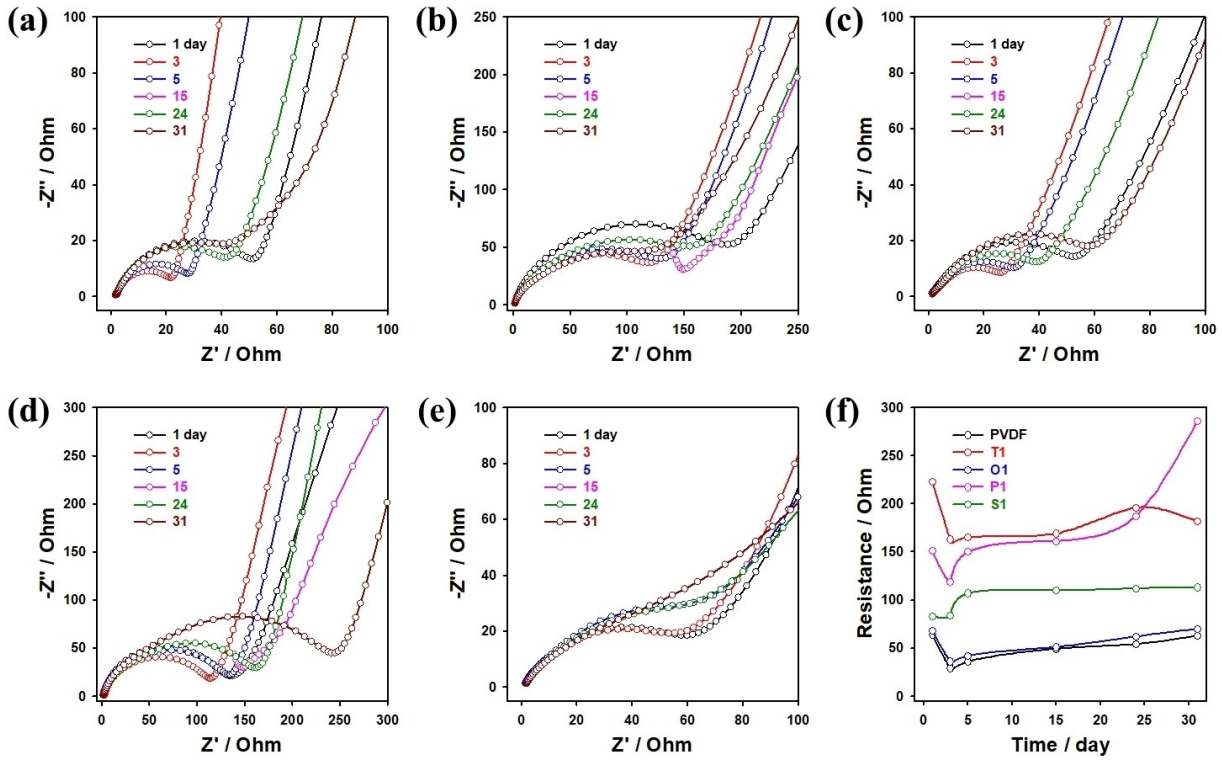

Figure 9. Nyquist plots of NCM811 cathode material for storage time of 31 days at 25 °C in the organic electrolyte of 1 M $LiPF_6$ in EC DEC (1 : 1, v/v) with (a) PVDF, (b) T1, (c) O1, (d) P1, (e) S1 binders and (f) resistance of binders *vs.* time.

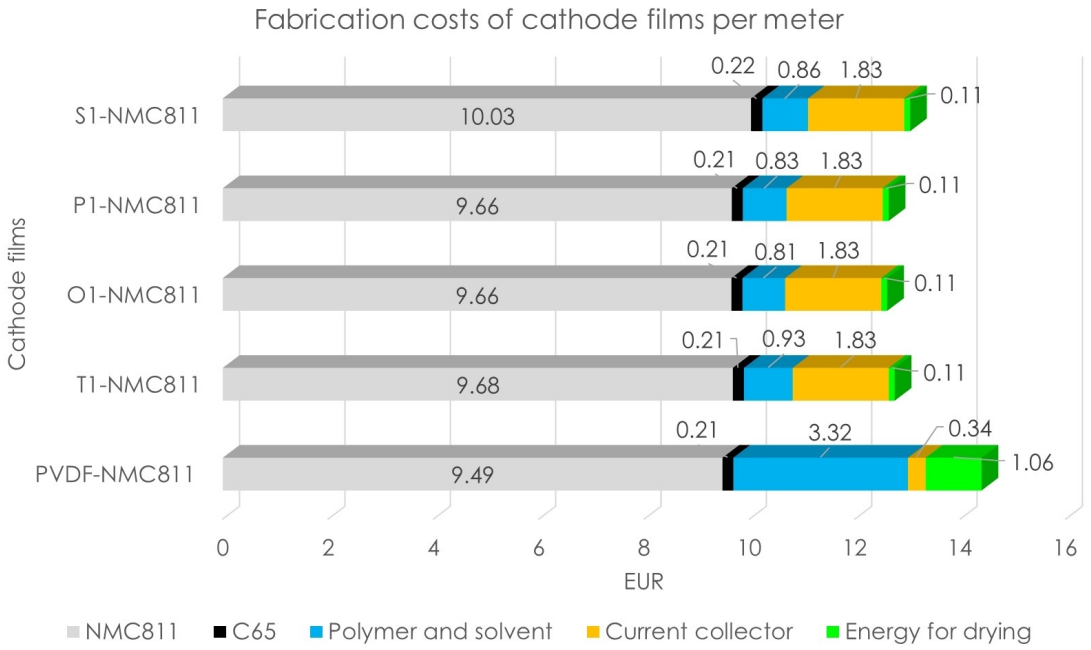

Figure 10. Cost comparison of NCM811 cathode films fabricated in this work with various binders (PVDF, T1, O1, P1, and S1) displaying the materials and energy costs.

manufacturing, which could potentially limit their large-scale application in energy storage. Recent research aims to find alternative battery systems such as sodium-ion batteries for large-scale applications.[66,67,68] Therefore, as demonstrated in this work, the use of more abundant raw materials and lower-cost fabrication of LIB components could provide some benefits in this regard. Of course, it should be noted that the application of the olefine and rubber-based alternative binders needs further investigation to improve and fully integrate into Li-ion battery chemistries. Furthermore, full economic evaluation is required to fully demonstrate the potential benefits of these binders from this perspective, which could provide further insight into their future potential for LIBs applications.

Conclusions

The obtained electrodes exhibit reasonable electrochemical performance due to the uniform distribution of particles and good adhesion to the current collector, maintaining stable cycle life due to less formation and attack of HF on NCM particles thanks to a stable formed SEI layer. In addition, the half cells maintained stable cycle life after different rate capabilities due to the facilitated lithium-ion diffusion and electronic conductivity. Binders used in olefine and rubber-based alternative binders help reduce the cost of electrode fabrication by almost half of the price of the PVDF-based cathodes, nevertheless, fabrication time is also reduced, and the cost is associated with the drying process. The fast evaporation of toluene allows discarding the slurry residues in a prompter manner avoiding prolonged exposure to solvent fumes. We can recommend these types of binders (usually used for the food/shoe industry) for the fabrication of conventional lithium battery electrodes, nevertheless, it needs to consider about processability and optimization of negative and positive electrode composite with these binders for maintaining stable and long-term electrochemical performance.

Declarations

- The authors have no relevant financial or non-financial interests to declare.
- The authors have no conflicts of interest to declare that are relevant to the content of this article.
- All authors certify that they have no affiliations with or involvement in any organization or entity with any financial interest or non-financial interest in the subject matter or materials discussed in this manuscript.
- The authors have no financial or proprietary interests in any material discussed in this article.

Author Contributions

Conceptualization: [A.T., A.B.], Methodology: [A.T., A.B., S.M.], General Experimental investigation and electrochemical analysis: [A.T., A.B., S.M.], Characterization XRD: [S.M.], Characterization SEM: [S.M.], Writing - original draft preparation: [A.T., A.B., S.M.], Writing - review and editing: [A.T., A.B., S.M., A.P., M.J.]

Acknowledgements

This work was supported by the financial support of the Austrian Federal Ministry for Climate Action, Environment, Energy, Mobility, Innovation, and Technology. The presented work was supported by the European Commission through the H2020 program under Grant agreement number 875028 (SUBLIME Project) and from the European Union's Horizon Europe program for research and innovation under grant agreement No. 101069686 (PULSELION project). Furthermore, the authors want to express their gratitude to Raad Hamid for the XRD measurements of obtained samples.

Conflict of Interests

The authors declare no conflict of interest.

Data Availability Statement

The data that support the findings of this study are available from the corresponding author upon reasonable request.

Keywords: high-energy lithium-ion batteries · binders · NCM811 · Ni-rich cathodes · fluorine-free binders · olefine and rubber-based polymers

[1] Y. Horowitz, C. Schmidt, D.-H. Yoon, L. M. Riegger, L. Katzenmeier, G. M. Bosch, M. Noked, Y. Ein-Eli, J. Janek, W. G. Zeier, C. E. Diesendruck, D. Golodnitsky, *Energy Technol.* **2020**, *8* (11), 2000580.
[2] J. B. Goodenough, Y. Kim, *Chem. Mater.* **2009**, *22*, 587–603.
[3] J. Meng, H. Guo, C. Niu, Y. Zhao, L. Xu, Q. Li, L. Mai, *Joule* **2017**, *1*, 522–547.
[4] A. Tron, Y. N. Jo, S. H. Oh, Y. D. Park, J. Mun, *ACS Appl. Mater. Interfaces* **2017**, *9*, 12391–12399.
[5] X. Su, Y. Xu, Y. Wu, H. Li, J. Yang, Y. Liao, R. Qu, Z. Zhang, *Energy Storage Mater.* **2023**, *56*, 642–663.
[6] S. Rana, R. C. Thakur, H. S. Dosanjh, *Solid State Ionics* **2023**, *400*, 116340.
[7] Z. Gao, L. Luo, R. Wen, X. Song, Z. Gao, Z. Zheng, J. Zhang, *J. Mater. Chem. A* **2023**, *11*, 1774–1784.
[8] K. Lee, S. Lim, A. Tron, J. Mun, Y.-J. Kim, T. Yim, T.-H. Kim, *RSC Adv.* **2016**, *6*, 101622–101625.
[9] J. Kim, H. Lee, H. Cha, M. Yoon, M. Park, J. Cho, *Adv. Energy Mater.* **2018**, *8*, 1870023.
[10] Y. K. Sun, S. T. Myung, B. C. Park, J. Prakash, I. Belharouak, K. Amine, *Nat. Mater.* **2009**, *8*, 320–324.
[11] G. V. Zhuang, G. Chen, J. Shim, X. Song, P. N. Ross, T. J. Richardson, *J. Power Sources* **2004**, *134*, 293–297.
[12] S. S. Zhang, *Ener. Stor. Mater.* **2020**, *24*, 247–254.
[13] P. Oh, B. Song, W. Li, A. Manthiram, *J. Mater. Chem. A* **2016**, *4*, 5839–5841.
[14] W. Dou, M. Zheng, W. Zhang, T. Liu, F. Wang, G. Wan, Y. Liu, X. Tao, *Adv. Funct. Mater.* **2023**, *33*, 2305161.
[15] G. J. Ross, J. F. Watts, M. P. Hill, P. Morrissey, *Polymer* **2000**, *41*, 1685–1696.
[16] A. C. Rolandi, C. Pozo-Gonzalo, I. de Meatza, N. Casado, D. Mecerreyes, M. Forsyth, *Adv. Ener. Sustainab. Res.* **2023**, *4*(12), 2300149.
[17] J. Li, Z. Wu, Y. Lu, Y. Zhou, Q. Huang, L. Huang, *Adv. Energy Mater.* **2017**, *7*, 1701185].
[18] X. Zhang, X. Ge, Z. Shen, H. Ma, J. Wang, S. Wang, L. Liu, B. Liu, L. Liu Y Zhao, *New J. Chem.* **2021**, *45*(22), 9846–9855.
[19] Solvay Specialty Polymers PVDF and the Other Fluorinated Polymers **2017**, https://www.solvay.com/sites/g/files/srpend221/files/2018-08/Sol-ef-PVDF-Design-and-Processing-Guide_EN-v2.7_0.pdf, Accessed 4th Mai 2024.
[20] H. Maleki, G. Deng, A. Anani, J. Howard, *J. Electrochem. Soc.* **1999**, *146*, 3224–3229.
[21] Z. Chen, L. Christensen, J. Dahn, *J. Electrochem. Soc.* **2003**, *150*, A1073–A1078.
[22] A. Du Pasquier, F. Disma, T. Bowmer, A. Gozdz, G. Amatucci, J. M. Tarascon, *J. Electrochem. Soc.* **1998**, *145*, 472–477.
[23] H. Wan, J. Xu, C. Wang, *Nat. Chem. Rev.* **2024**, *8*, 30–44.
[24] https://echa.europa.eu/hot-topics/perfluoroalkyl-chemicals-pfas, Accessed 3rd May **2024**.
[25] G. B. Xia, L. Cao, G. L. Bi, *J. Power Sources* **2017**, *367*, 90–105.
[26] D. Bresser, D. Buchholz, A. Moretti, A. Varzi, S. Passerini, *Energy Environ. Sci.* **2018**, *11*, 30963127.
[27] J. E. Marshall, A. Zhenova, S. Roberts, T. Petchey, P. Zhu, C. E. Dancer, V. Goodship, *Polymer* **2021**, *13*(9), 1354.
[28] https://echa.europa.eu/documents/10162/13579/rac_joint_nmp_opinion_en.pdf/e4b4f43b-a3bd-a7c0-08be-16c3886593e7, Accessed 3rd May **2024**.
[29] R. Lohmann, I. T. Cousins, J. C. DeWitt, J. Glüge, G. Goldenman, D. Herzke, A. B. Lindstrom, M. F. Miller, C. A. Ng, S. Patton, M. Scheringer, X. Trier, Z. Wang, *Sci. Technol.* **2020**, *54* (20), 12820–12828.
[30] Y. Guo, X. Li, Z. Wang, H. Guo, J. Wang, F. Meng, G. Yan, *Mater. Today Sustain.* **2023**, *21*, 100304.
[31] Y. T. Malik, S.-Y. Shin, J. I. Jang, H. M. Kim, S. Cho, Y. R. Do, J.-W. Jeon, *Small* **2023**, *19*, 2206141.
[32] Z. Wu, Z. Wan, Z. Li, Q. Du, T. Wu, J. Cao, M. Ling, C. Liang, Y. Tan, *Small* **2023**, *19*, 2205065.
[33] Y. Y. Hwang, J. H. Han, S. H. Parka, Y. J. Lee, *J. Mater. Chem. A* **2023**, *11*, 14086–14095.
[34] X. Hu, K. Liu, S. Zhang, G. Shao, S. Ravi P Silva, P. Zhang, *Nano Res.* **2023**, *17*, 2790–2799.
[35] J.-H. Lee, J. Kim, M. H. Jeong, K. H. Ahn, H. L. Lee, H. J. Youn, *J. Power Sources* **2023**, *557*, 232552.
[36] L. Yu, X. Liu, S. Feng, S. Jia, Y. Zhang, J. Zhu, W. Tang, J. Wang, J. Gong, *Chem. Eng. J.* **2023**, *476*, 146733.
[37] M. A. Kebede, *Curr. Opin. Electrochem.* **2023**, *29*, 101261.
[38] F. Peng, L. Zhang, G. Yang, Y. Li, Q. Pan, Y. Li, S. Hu, F. Zheng, H. Wang, Q. Li, *Chem. Eng. J.* **2023**, *451*, 138911.
[39] S. Ma, X. Zhang, S. Wu, E. Fan, J. Lin, R. Chen, F. Wu, L. Li, *Energy Storage Mater.* **2023**, *55*, 556–565.
[40] M. Akhilash, P. S. Salini, B. John, S. Sujatha, T. D. Mercy, *Chem. Rec.* **2023**, *23*, e2023001.
[41] S. She, Y. Zhou, Z. Hong, Y. Huang, Y. Wu, *ACS Appl. Energ. Mater.* **2023**, *6* (13), 7289–7297.
[42] Z. Xie, J. He, Z. Xia, Q. Cai, Z. Tang, J. Cai, Y. Chen, X. Li, Y. Fan, L. Xing, Y. Shen, W. Li, *J. Energy Chem.* **2023**, *86*, 197–207.
[43] Y. Wang, H. Du, G. Tian, Z. Liu, B. Wang, *Solid State Ionics* **2023**, *399*, 116290.
[44] X. Deng, R. Zhang, K. Zhou, Z. Gao, W. He, L. Zhang, C. Han, F. Kang, B. Li, *Energy Environ. Mater.* **2023**, *6*, e12331.
[45] Y.-J. Lee, S.-B. Hong, D.-W. Kim, *J. Ind. Eng. Chem.* **2023**, *122*, 341–348.
[46] Y. B. Song, K. H. Baeck, H. Kwak, H. Lim, Y. S. Jung, *Adv. Energy Mater.* **2023**, *13*, 2301142.
[47] A. Mills, G. Yang, W.-Y. Tsai, X. C. Chen, R. L. Sacci, B. L. Armstrong, D. T. Hallinan Jr, J. Nanda, *J. Electrochem. Soc.* **2023**, *170*, 080513.
[48] A. Tron, R. Hamid, N. Zhang, A. Paolella, P. Wulfert-Holzmann, V. Kolotygin, P. Lopez-Aranguren Oliver, *J. Energy Storage* **2023**, *66*, 107480.
[49] X. Zhou, Q. Ye, B. Pang, Z. Wu, T. Yang, W. Zhang, Y. Xia, H. Huang, X. Xia, X. He, Y. Gan, J. Zhang, *ACS Appl. Energy Mater.* **2023**, *23(6)*, 12120–12127.
[50] M. Kim, J. Seo, J. P. D. Suba, K. Y. Cho, *Mater. Chem. Front.* **2023**, *7*, 5475–5499.
[51] A. Tron, R. Hamid, N. Zhang, A. Beutl, *Nanomaterials* **2023**, *13*, 327.
[52] W. Huang, W. Wang, Y. Wang, Q. Qu, C. Jin, H. Zheng, *J. Mater. Chem. A* **2021**, *9*, 1541–1551.
[53] D. H. S. Tan, E. A. Wu, H. Nguyen, Z. Chen, M. A. T. Marple, J. M. Doux, X. Wang, H. Yang, A. Banerjee, Y. S. Meng, *ACS Energy Lett.* **2019**, *4*, 2418–2427.
[54] M. Zhang, P. Zhang, W. Wen, H. Wang, B. He, Y. Gong, J. Jin, R. Wang, *Coatings* **2022**, *12*, 1964.
[55] Q. Liu, Y. Sun, S. Wang, Q. An, L. Duan, G. Zhao, C. Wang, K. Doyle-Davis, H. Guo, X. Sun, *Mater. Today* **2023**, *64*, 21–30.

[56] X. Zheng, Z. Cao, W. Luo, S. Weng, X. Zhang, D. Wang, Z. Zhu, H. Du, X. Wang, L. Qie, H. Zheng, Y. Huang, *Adv. Mater.* **2023**, *35*, 2210115.
[57] A. Tron, Y. D. Park, J. Mun, *Solid State Sci.* **2020**, *101*, 106152.
[58] K. Mao, Y. Yao, Y. Chen, W. Li, X. Shen, J. Song, H. Chen, W. Luan, K. Wu, *J. Energy Storage* **2024**, *84*, 110807.
[59] B. Zhu, H. Li, Y. Ning, Z. Yu, L. Meng, G. Wei, J. Qu, *J. Mater. Chem. A* **2024**, *12*, 6527–6538.
[60] Y. Komoda, K. Ishibashi, K. Kuratani, K. Suzuki, N. Ohmura, H. Kobayashi, *J. Power Sources* **2023**, *568*, 232983.
[61] Z. H. Xie, M. Z. Rong, M. Q. Zhang, *ACS Appl. Mater. Interfaces* **2013**, *13*, 28737–28748.
[62] B. Wang, J. Ni, J. Li, J. Wang, Q. Zhang, Y. Chen, C. Lai, Y. Feng, *Ionics* **2021**, *27*, 3749–3760.
[63] J. Lai, J. Zhang, Z. Li, Y. Xiao, W. Hua, Z. Wu, Y. Chen, Y. Zhong, W. Xiang, X. Guo, *Chem. Commun.* **2020**, *56*, 4886–4889.
[64] F. Wu, N. Liu, L. Chen, Y. Su, G. Tan, L. Bao, Q. Zhang, Y. Lu, J. Wang, S. Chen, J. Tan, *Nano Energy* **2019**, *59*, 50.
[65] J. Yang, Y. Xia, *ACS Appl. Mater. Interfaces* **2016**, *2*(8), 1297–1308.
[66] Y. Zhao, Y. Kang, J. Wozny, J. Lu, H. Du, C. Li, T. Li, F. Kang, N. Tavajohi, B. Li, *Nat. Rev. Mater.* **2023**, *8*, 623–634.
[67] A. N. Singh, M. Islam, A. Meena, M. Faizan, D. Han, C. Bathula, A. Hajibabaei, R. Anand, K.-W. Nam, *Adv. Funct. Mater.* **2023**, *23*, 2304617.
[68] K. Sada, J. Darga, A. Manthiram, *Adv. Energy Mater.* **2023**, *13*, 2302321.

Manuscript received: August 1, 2024
Version of record online: September 24, 2024